Pergamon

Scripta Materialia, Vol. 40, No. 7, pp. 801–808, 1999
Elsevier Science Ltd

1359-6462/99/$–see front matter

PII S1359-6462(99)00013-5

HIGH-STRAIN-RATE DEFORMATION OF PURE ALUMINUM REINFORCED WITH 25% ALUMINA SUBMICRON PARTICLES NEAR THE SOLIDUS TEMPERATURE

B. Q. Han, S. R. Agnew, and D. C. Dunand
Department of Materials Science and Engineering, Northwestern University, Evanston, IL 60208

(Received December 18, 1998)
(Accepted January 7, 1999)

Introduction

Discontinuously reinforced aluminum metal matrix composites (MMCs) with about 20 vol.% reinforcement produced by powder metallurgy (PM) are attractive for many structural applications because of their high specific strength and stiffness. While they exhibit reduced ductility and toughness at room temperature, many of them can be superplastically deformed at high-strain rates in the vicinity of their solidus temperature [1–8].

Recently, the mechanical properties at room and elevated temperatures of dispersion-strengthened-cast aluminum (DSC-Al) with high volume fractions (>25 vol.%) of submicron Al_2O_3 oxide dispersoids have been investigated [9,10]. The material has characteristics of both Al-MMCs (e.g., high modulus, strength, and low coefficient of thermal expansion) and conventional PM oxide-dispersion-strengthened aluminum with lower reinforcement content (e.g., high creep resistance). While the room-temperature ductility of DSC-Al is quite high (9.4% for extruded DSC-Al with 25 vol.% Al_2O_3 oxide particles [9]), its formability at elevated temperatures is limited by its high creep strength and low creep ductility [10,11]. Because of the similarity of microstructure between DSC-Al and other Al-MMCs, the question arises whether DSC-Al containing 25% Al_2O_3 particles can exhibit high-strain-rate superplasticity near the solidus temperature. The purpose of the present note is to investigate this issue.

Material and Procedure

The material used in this and previous studies [9–11] was DSC-Al fabricated by liquid metal pressure infiltration by Chesapeake Composite Corp. (New Castle, DE). DSC-Al consists of pure aluminum (>99.9%) reinforced with 25 vol.% of submicron α-Al_2O_3 dispersoids with a mean diameter of 0.28 ± 0.03 μm. After infiltration, DSC-Al was extruded at 823 K with an extrusion ratio of 12, resulting in a very fine grain size of about 1.3 μm which is stable up to 923 K (grains were found to grow to only 1.8 μm after 139 h at that temperature [9]). The solidus temperature of extruded DSC-Al was measured as 926.6 K (Fig. 1) by a DuPont 2100 Differential Thermal Analysis (DTA) instrument, with heating rate of 20 K/min to 673 K and 5 K/min to 973 K. For comparison, the solidus temperature of annealed 99.999% pure aluminum from Johnson Mathey, Co. (Ward Hill, MA) was measured under the same

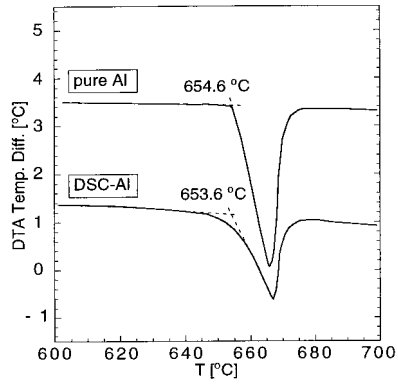

Figure 1. DTA curves for DSC-Al and pure aluminum.

conditions as 927.6 K, suggesting that the higher grain and interface boundary areas in DSC-Al have an insignificant effect on the solidus temperature.

Tensile specimens were machined along the extrusion direction with a gage diameter of 5.0 mm and a gage length of 14.0 mm (two of the specimens had a gage diameter of 4.0 mm and gage length of 16.9 mm). After heating to the test temperature in 50 minutes and soaking at that temperature for 30 minutes, tensile tests were conducted in air using a MTS 8100 servohydrautic load frame at constant cross-head velocities V with initial strain rates $\dot{\varepsilon}_o$ between $7.4 \cdot 10^{-3}$ s^{-1} and 2.5 s^{-1} at temperatures of 913 K or 923 K.

The fracture surfaces of tested specimens were observed using a Hitachi S-570 Scanning Electron Microscope (SEM) operating at 20 kV. A semiautomatic method of grain orientation determination [12] was employed using a Hitachi 8100H Transmission Electron Microscope (TEM) operating at 200 kV. The method requires a double tilt holder and, for such small grain sizes, convergent beam capability. Kikuchi electron diffraction patterns were used to gather orientation data calculated as **g** (a 3×3 rotation matrix for relating crystal axes to sample axes). Subsequently, the misorientation was calculated between each pair of neighboring grains A and B as $\mathbf{R}_{AB} = \mathbf{g}_B \cdot \mathbf{g}_A^{-1}$ or, equivalently, as an angle/axis pair. Only the lowest misorientation angle (disorientation) is reported in the current study. For preparation of TEM samples, disks with a diameter of 3 mm were punched with their planes in the extrusion direction, dimpled, polished to a thickness of about 20 μm, and thinned to perforation by ion milling. To assess the integrity of the Al_2O_3/Al bonding, ultrasonic modulus measurements were made. Shear and longitudinal waves were produced by Matec quartz piezoelectric transducers operating at 20 MHz and 50 MHz, respectively. The velocity of ultrasonic waves propagating through the samples was determined using a pulse-echo technique with a digital oscilloscope. Sample density was measured in de-ionized water according to Archimedes' principle at room temperature.

Experimental Results

Initial strain rate, tensile fracture elongation and failure time of DSC-Al tested at temperatures of 14 K and 4 K below the solidus temperature are listed in Table 1. The elongations near the solidus temperature are higher than the elongations at room temperature [9] or under creep conditions [10,11], but far short of superplastic values. Fig. 2 shows the true strain dependence of the true stress and instantaneous strain rate of DSC-Al tested at an initial strain rate of 2.5 s^{-1} at 913 K. This figure shows that after initial deformation, the flow stress and the strain rate decrease with increasing strain. Fig. 3

TABLE 1
Initial Strain Rate $\dot{\varepsilon}_o$, Elongation to Failure δ ($=\Delta 1/1_0 \cdot 100$) and Failure Time t_f of Extruded DSC-Al at 913 K ($T/T_s = 0.985$) and 923 K ($T/T_s = 0.996$)

	913 K						923 K
$\dot{\varepsilon}_o$ [s^{-1}]	$7.4 \cdot 10^{-3}$	$1.8 \cdot 10^{-2}$	$7.1 \cdot 10^{-2}$	$2.3 \cdot 10^{-1}$	$7.1 \cdot 10^{-1}$	2.5	$7.0 \cdot 10^{-3}$
δ [%]	15.3	31*	19.3	33.6*	14.3	17.1	17.9
t_f [s]	20.45	17.16	2.60	1.36	0.18	0.07	2.43

* specimens with a smaller gage diameter and a longer gage length.

shows the relationship between flow stress and true strain rate measured at a true strain of 0.04. The stress exponent increases from n = 1.7 in the low-stress regime to n = 6.9 in the high-stress regime.

Fig. 4 shows the initial strain rate $\dot{\varepsilon}_o$ as a function of rupture time t_f and of rupture time divided by failure strain ε_f($=\delta/100$). As for DSC-Al tested under creep conditions between 608 K and 773 K [11], the data in Figure 4 can be successfully fitted to the Monkman-Grant relation:

$$t_f \cdot \dot{\varepsilon}_o^{\,m} = C \tag{1}$$

where m = 1.035 and C = 0.182, and to the modified Monkman-Grant relation:

$$\frac{t_f}{\varepsilon_f} \cdot \dot{\varepsilon}_o^{\,m'} = C' \tag{2}$$

where $m' = 1.005$ and $C' = 0.963$.

Fracture surfaces of DSC-Al at 913 K are shown in Fig. 5 for the lowest and highest strain rates used. Although some oxide particles appear on fracture surfaces in both cases, no dimples are observed. Due to insufficient plastic deformation of the matrix, most of the submicron alumina particles still remain in the matrix. However, matrix flow seems more pronounced at the lower strain rate.

The grain boundary misorientations were analyzed based on 40 separate grain orientations resulting in 55 mutual misorientation measurements, using an extruded DSC-Al sample crept at a stress of 32.9 MPa and at a temperature of 673 K [10,11]. The grain boundary disorientation distribution is plotted in Fig. 6 which shows that low-angle grain boundaries of less than 20° are relatively rare (only about 21%), and that high-angle grain boundaries are dominant. Furthermore, given the small number of

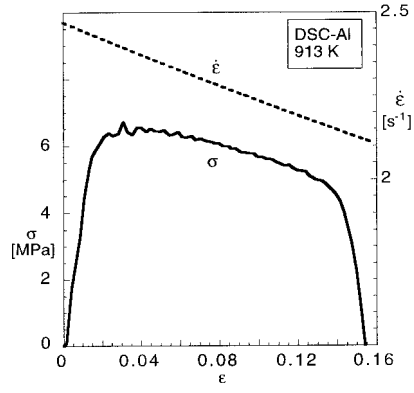

Figure 2. True strain dependence of true stress and instantaneous strain rate of DSC-Al for an initial strain rate of 2.5 s^{-1} at 913 K.

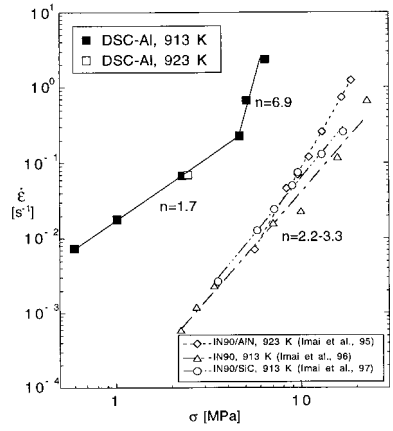

Figure 3. Strain rate *vs.* stress of DSC-Al and other superplastic unalloyed aluminum materials [15–17] at temperatures slightly below the solidus temperature.

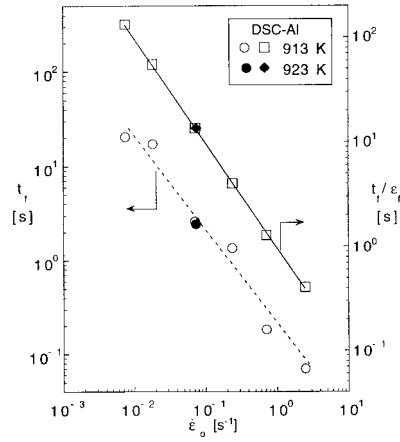

Figure 4. Initial strain-rate dependence of rupture time and rupture time divided by rupture strain for DSC-Al.

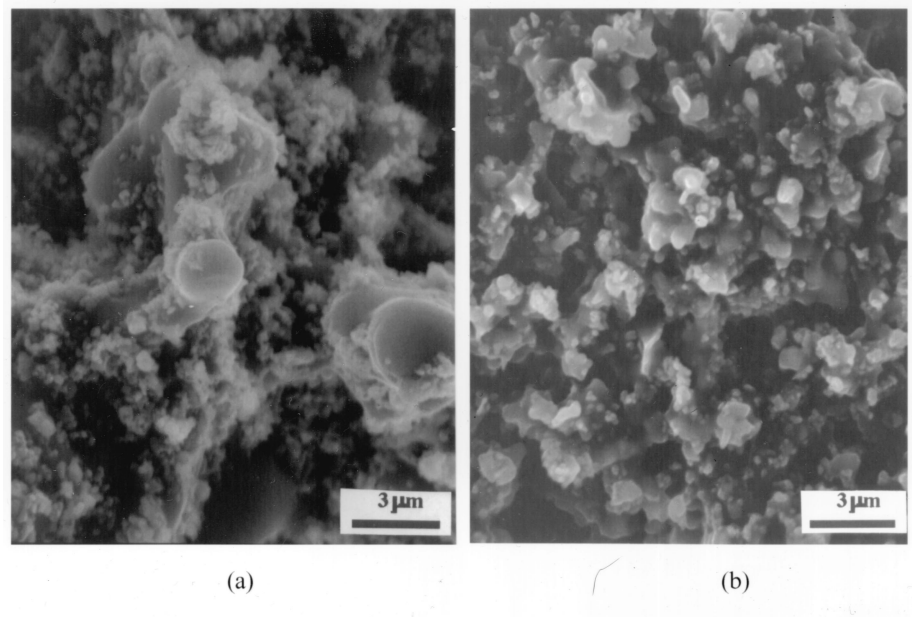

Figure 5. Tensile fracture surfaces of DSC-Al deformed at 913 K at strain rates of (a) $7.4 \cdot 10^{-3}$ s^{-1} and (b) 2.5 s^{-1}.

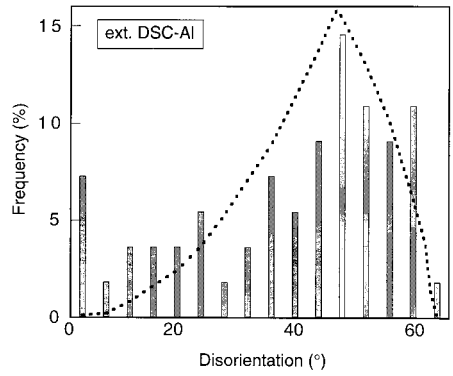

Figure 6. Distribution of grain boundary disorientation for extruded DSC-Al determined by TEM, and random distribution (dashed line) [13].

measurements, it cannot be concluded that the measured distribution strongly deviates from the random distribution derived by Mackenzie [13] and shown as a dashed line.

The Young's modulus of the DSC-Al was measured to be 107 GPa ($\pm$1%) by the ultrasonic pulse-echo method. This value is quite similar to that found previously in DSC-Al-2.5% Mg containing 25% Al_2O_3 [9], and within the bounds of Hashin & Shtrikman [14], indicating good interface bond integrity. Since the density was found to be 3.00 g/cm^3 (99.4% theoretical density, assuming exactly 25 vol% Al_2O_3), the effect of porosity was ignored.

Discussion

Microstructural characteristics, processing, test conditions and tensile properties are listed in Table 2 for DSC-Al, several superplastic MMCs with a similar volume fraction of reinforcement, and superplastic pure aluminum. Table 2 shows that: (i) all the materials were extruded and had a recrystallized microstructure with a very fine stable grain size; (ii) the volume fractions of reinforcement in the MMCs were similar, from 15 to 25%; (iii) the ratio of grain size to particle sizes was similar, from 1 to 5; (iv) the test temperatures were similar, very high and close to the solidus temperature; (v) the strain rates were in the range of high-strain-rate superplasticity. However, despite these similarities, DSC-Al does not show superplasticity; this observation is discussed in the following.

It is generally accepted that grain boundary sliding and interfacial sliding are the controlling deformation mechanisms for high-strain-rate superplasticity [18,19]. The grains in superplastic MMCs are usually very fine and separated by high-angle grain boundaries. As shown in Fig. 6, the grain orientation in DSC-Al is close to random and thus meets the requirements for grain boundary sliding, although there is a certain fraction of very low angle boundaries which likely formed during creep deformation of the sample. Therefore, neither matrix grain size nor matrix grain boundary character in DSC-Al can explain the lack of superplasticity. In addition, a liquid phase in the matrix is often a sufficient [1,8], but not always a necessary, requirement for high-strain-rate superplasticity, as shown in Table 2. In fact, the maximum elongation is usually observed at temperatures below the solidus temperature [6]. We thus conclude that the testing temperature is not the reason for the lack of high-strain-rate superplasticity observed in DSC-Al.

Even though the size and volume fraction of particles for DSC-Al are similar to those for superplastic MMCs listed in Table 2, a major difference is the nature of the reinforcing ceramic (Al_2O_3 vs. SiC, Si_3N_4 and AlN). It has been noted that aluminum will form a strong bond with SiC [20], Si_3N_4 and

TABLE 2
Comparison of DSC-Al with Several Particulate Reinforced Aluminum Composites Deformed at High-Strain-Rate Superplastic Conditions

Matrix	Particles (vol.%)	Processing*	d_m (μm)	d_r (μm)	d_m/d_r	T (K)	T/T_s	$\dot{\varepsilon}_o$ (s^{-1})	n	δ_{max} (%)	Ref.
Pure Al	25% Al_2O_3	cast+ext.(12)	1.3	0.28	4.6	913 −923	0.985 −0.996	0.007 −2.5	1.7 −6.9	34	Present work
6061Al	20% Si_3N_4	PM+ext.(100)	1	0.2	5	833	1.004	2	2–3	620	[2]
6061Al	20% Si_3N_4	PM+ext.(100)	1.9	0.5	3.8	833	1.005	2	2	500	[3]
5052Al	20% Si_3N_4	PM+ext.(100)	1	0.2	5	818	0.986	1	2–3	700	[4]
2124Al	20% Si_3N_4	PM+ext.(100)	1	0.2	5	773	0.979	0.3	3	280	[5]
pure Al (IN90)	15% AlN	PM+ext.(44) +rolling	2	1.8	1.1	913	0.979	0.002	2.2	200	[15]
Pure Al - (IN90)		PM+ext.(44) +rolling	2	—	—	913	0.979	0.02	2.5	400	[16]
pure Al (IN90)	15% SiC	PM+ext.(44) +rolling	2	2	1	913	0.979	0.01	3.3	200	[17]

* Values in parentheses are extrusion ratio.

Al_2O_3 [21]. There are indications that interface products form at the SiC/Al [20] and Si_3N_4/Al [21] interfaces. These are typically nanocrystalline or amorphous compounds like SiO_2 or Al_4C_3 in the case of SiC, and AlN in the case of Si_3N_4. It is also well known that if the matrix is an alloy, segregation will occur due to interfacial strains and more complex interfacial reaction products (such as spinel) may also form. It is reasonable to suggest that the interfacial sliding or incipient melting [22] often required for superplastic elongation is assisted by the presence of these interface reaction products. In the case of pure Al and pure Al_2O_3, the observed lack of interfacial products [21] may provide an explanation for the poor ductility observed in the current study. In other words, if the bonding is strong with no interfacial reaction products, the potential for sliding may be minimal. We are aware of only one aluminum composites reinforced with 19 vol.% Al_2O_3 for which an elongation of 135% was reported at a relatively low temperature of 803 K and at a low strain rate of $7 \cdot 10^{-4}$ s^{-1} [23]. However, the matrix of this composite was the magnesium-containing 6061Al alloy and exhibited most likely reaction products at interfaces, which may have assisted interfacial sliding.

A second difference between DSC-Al and the superplastic Al-MMCs in Table 2 is the extrusion ratio, which affects the distribution of particles and thus the superplastic properties of Al-MMCs. For example, a 6061Al composite with uniformly-distributed 20 vol.% SiC whiskers exhibited high-strain-rate superplasticity in Ref. [7], while the same nominal composite with many whisker-rich and -poor bands did not show superplasticity in Ref. [18]. This effect may also be important in DSC-Al with a distribution of particles which is most probably not as uniform as for the Al-MMCs in Table 2, given the large difference in extrusion ratio (12 and 44–100, respectively).

A third major difference between DSC-Al and the superplastic Al-MMCs in Table 2 is the processing route. The latter materials were made by PM processing, where aluminum powders with an initial size of about 40 μm densified and recrystallized into fine matrix grains with large-angle boundaries during pressure sintering and subsequent extrusion. These matrix grains contain well-distributed ultra-fine incoherent oxide particles (with a volume fraction of less than 0.6 vol.% and an average size less than 20 nm, and originating from the oxidized aluminum powders [24]), which may inhibit dislocation movement in the matrix such that grain boundary sliding may be the dominant matrix deformation mechanism. On the other hand, DSC-Al materials in this investigation were made by pressure casting and subsequent extrusion and thus did not contain such ultra-fine oxide particles. As

expected, DSC-Al deforms much faster than superplastic PM pure aluminum and aluminum MMCs (Fig. 3). While the strain exponent is about $n = 2 \sim 3$ in superplastic pure aluminum and Al-MMCs where the deformation mechanisms are grain boundary sliding and interfacial sliding, the stress exponent in DSC-Al changes from $n = 2$ to $n = 7$, suggesting that the controlling deformation mechanisms are diffusional creep in the low-stress regime and dislocation creep in the high-stress regime.

It is noteworthy that plots of initial strain-rate vs. rupture time or rupture strain-normalized rupture time (Fig. 4) can be described by the well-known Monkman-Grant relations (Eqs. (1) and (2)) which hold for DSC-Al and Al-MMCs deforming by creep at lower temperatures under constant load conditions [11]. However, the present experiments were conducted at constant cross-head velocity, so that the constants in Eqs. (1) and (2) are expected to be different. At constant load and for $m = 1$ and $m' = 1$, these constants (relabelled with subscript 1) are predicted to be $C_1 = 1/n$ and $C_1' = \varepsilon_2/\varepsilon_f$ [11], where n is the stress exponent and ε_2 is the strain accumulated during secondary steady state creep. Therefore, C_1 is always less than unity and C_1' is about 0.5 for constant-load creep tests [11]. On the other hand, for tensile tests with constant cross-head velocities, $\dot{\varepsilon}_0 = V/1_0$ (where 1_0 is the initial gage length), $\varepsilon_f = \Delta 1/1_0$ and $\Delta 1 = V \cdot t_f$ (where $\Delta 1$ is the displacement to failure). With these definitions and $m = m' = 1$, Eqs. (1) and (2) can be both rewritten as:

$$t_f \cdot \dot{\varepsilon}_0 = \varepsilon_f. \tag{3}$$

For materials deforming by creep deformation mechanisms, ε_f is usually small and reasonably constant, so Eq. (3) predicts that t_f and $\dot{\varepsilon}_0$ are inversely proportional. In superplastic materials, ε_f exhibits a maximum at an optimal strain rate, such that t_f and $\dot{\varepsilon}_0$ do not follow the Monkman-Grant relation. Therefore, the inverse relationship between $\dot{\varepsilon}_0$ and t_f in Fig. 4 is further indirect evidence that DSC-Al deformed by creep mechanisms and not by superplastic mechanisms. In contrast, the inverse relationship between $\dot{\varepsilon}_0$ and t_f/ε_f (in Fig. 4 and Eq. (2)) cannot be used as evidence of lack of superplasticity, because Eq. (3) is always valid for tensile tests with constant cross-head velocities independently of the deformation mechanisms.

Conclusions

High-temperature tensile tests were performed on dispersion-strengthened-cast unalloyed aluminum (DSC-Al) at temperatures 14 K and 4 K below the solidus temperature and at strain rates between $7.4 \cdot 10^{-3}$ s^{-1} and 2.5 s^{-1}. As compared to Al-MMCs exhibiting high-strain-rate superplasticity, DSC-Al shows similar matrix composition, grain size, grain boundary orientation, particle size and particle volume fraction; however, high-strain-rate superplasticity is not observed in DSC-Al at similar test temperatures and strain rates. Three explanations are advanced to explain this observation. First, lack of interfacial reaction in DSC-Al may be unfavorable for interfacial sliding. Second, relatively low extrusion ratio for DSC-Al may lead to a not fully uniform distribution of particles, which is known to inhibit high-strain-rate superplasticity. Third, DSC-Al (processed by casting) does not contain ultra-fine oxide particles typical of powder-metallurgy composites, so that dislocation and diffusional creep may be favored in DSC-Al, as opposed to grain boundary sliding observed in PM composites. The stress exponent and the similarity of the strain-rate dependence of rupture time with the Monkman-Grant creep relation are further indications that the deformation in DSC-Al is controlled by creep, not by superplastic, deformation mechanisms.

Acknowledgments

Financial support from the National Science Foundation under grant No. DMR 9417636 (Dr. Bruce McDonald monitor) is gratefully acknowledged. Discussions with Dr. Rahul Mitra (Northwestern University) on interfacial issues were very helpful.

References

1. T. G. Nieh, C. A. Henshall, and J. Wadsworth, Scripta Metall. 18, 1405 (1984).
2. M. Mabuchi, K. Higashi, Y. Okada, S. Tanimura, T. Imai, and K. Kubo, Scripta Metall. Mater. 25, 2517 (1991).
3. H. Iwasaki, M. Yakeuchi, T. Mori, M. Mabuchi, and K. Higashi, Scripta Metall. Mater. 31, 255 (1994).
4. M. Mabuchi and K. Higashi, Mater. Sci. Eng. Al79/Al80, 625 (1994).
5. M. Mabuchi, K. Higashi and T. G. Langdon, Acta Metall. Mater. 42, 1739 (1994).
6. B. Q. Han and K. C. Chan, Mater. Sci. Eng. A212, 256 (1996).
7. B. Q. Han and K. C. Chan, Scripta Mater. 36, 593 (1997).
8. M. Mabuchi and K. Higashi, JOM. June, 34 (1998).
9. A. M. Redsten, E. M. Klier, A. M. Brown, and D. C. Dunand, Mater. Sci. Eng. A201, 88 (1995).
10. A. M. Jansen and D. C. Dunand, Acta Mater. 45, 4583 (1997).
11. D. C. Dunand, B. Q. Han, and A. M. Jansen, Metall. Mater. Trans. A. in press (1999).
12. Q. Liu, J. Appl. Crystallogr. 27, 755 (1994).
13. J. K. Mackenzie, Biometrika. 45, 229 (1958).
14. Z. Hashin and S. Shtrikman, J. Mech. Phys. Solids. 11, 127 (1963).
15. T. Imai, G. L'Esperance, B. D. Hong, and S. Kojima, Scripta Metall. Mater. 33, 1333 (1995).
16. T. Imai, S. Kojima, G. L'Esperance, B. D. Hong, D. Jiang, and T. G. Nieh, Scripta Mater. 35, 1189 (1996).
17. T. Imai, S. Kojima, and D. Jiang, Mater. Sci. Eng. A225, 184 (1997).
18. T. G. Nieh and J. Wadsworth, Mater. Sci. Eng. Al47, 129 (1991).
19. B. Q. Han, K. C. Chan, T. M. Yue, and W. S. Lau, Scripta Mater. 33, 925 (1995).
20. R. J. Arsenault, Composites. 25, 540 (1994).
21. M. Naka, Ultramicroscopy. 39, 128 (1991).
22. H.-G. Jeong, K. Hiraga, M. Mabuchi, and K. Higashi, Acta Mater. 46, 6009 (1998).
23. W. Zheng, J. Yun, A. Ma, J. Jiang, and R. S. Tan, Mater. Sci. Forum. 243–245, 511 (1997).
24. Y.-W. Kim, W. M. Griffith and F. H. Froes, JOM. 27 (1985).